Whole-Teflon Lab on a Film

Zhenghao Wang[a], Yilin Yin[a], and Hongkai Wu[a,b,*]

[a] *Department of Chemistry, The Hong Kong University of Science and Technology, Clear Water Bay, Kowloon, Hong Kong, China*

[b] *The Hong Kong Branch of Chinese National Engineering Research Centre for Tissue Restoration, The Hong Kong University of Science and Technology, Clear Water Bay, Kowloon, Hong Kong, China*

*Email: chhkwu@ust.hk

ABSTRACT: This study presents a convenient and cost-effective technology for fabricating flexible thin-film, integrative whole-Teflon microfluidic chips. By employing micro embossing techniques, we created micropatterns on a thin FEP film (~50 μm), which were then sealed with another flat FEP thin film (~200 μm) to form microchannels. This approach enables rapid prototyping of lab-on-a-film FEP microchips using minimal equipment and at a low cost. Our microfluidic chip stands out due to two key factors: one is inherited from the Teflon material, and the other is that the entire microchip is a very thin film. The combination of these factors provides distinct advantages, including exceptional chemical resistance, high transparency and flexibility, and efficient heat transfer. We developed an adhesive-free, tight-fit, and solvent-resistant interconnector to interface the FEP thin-film microdevices with the macroscopic world for stable fluid delivery. Microvalves are integrated into our Teflon microfluidic film chips, which are easy to operate for fluid manipulation. As a proof of concept, we demonstrated the versatility and enhanced performance of our transparent FEP microfluidic film chips through an on-chip photochemical reaction. These FEP microfluidic film chips offer powerful and diverse features that expand the capabilities of microfluidics, making them an attractive option for a wide range of applications such as biosensing, portable detection, wearable electronics, and organic reactions.

1. INTRODUCTION

Microfluidics is a rapidly evolving technology with tremendous potential for miniaturizing and integrating laboratory functions for the purification, synthesis, or analysis of chemical and biological compounds[1–4]. Traditional lab-on-a-chip microdevices consist of plates of substrates with a thickness (several millimeters) greater than the microchannels (below 1 mm). These microchips can be fabricated from thick slabs of various materials[5,6], including glass and silicon, elastomers (e.g., PDMS), and polymers (e.g., polycarbonate or polymethylmethacrylate). However, conventional bulk-based microchips are mechanically stiff and possess low flexibility. As an alternative, thin film-based microchips made of flexible polymer films, typically less than 500 μm thick[7], have recently emerged with several advantages over bulk counterparts. Thin microfluidic chips offer high flexibility, allowing them to be easily bent, wrapped around, and folded. They provide several distinct benefits: (1) fast and efficient heat transfer through the thin films for accurate temperature control in on-chip chemical and biological reactions[8], (2) flexibility enabling efficient morphological response to the environment[9], facilitating the integration of pumps and valves for fluid control, (3) reduced chip cost due to minimal chip volume[10] and (4) compatibility with mass production. Film-based microfluidic chips have been developed using various materials, including paper[11], PDMS[12], plastic films[13], and photocurable polymers[14]. The fabrication of lab-on-a-film systems requires the patterning of microchannel structures on the thin films. For example, Truckenmüller et al.[15] achieved high-resolution thermoforming of thin polymer films using a modified hot embossing process incorporating vacuum and blow assistance. Specifically, the polycarbonate, polystyrene, and cycloolefin films were affixed to the designated mold by applying vacuum or blowing techniques, allowing for the formation of micropatterns once heated. Ikeuchi et al.[16,17] developed the membrane micro-embossing (MeME) process to fabricate 3D microdevices made of thin PLA films. During the pressurization, the PLA is deformed to conform to the mold's surface with backpressure from the support paraffin substrate. Alternatively, Hu et al.[13] developed a one-step strategy for rapidly fabricating plastic film-based microfluidic chips. The microchannels are formed by the spontaneous rising of the thermally expanding polyethylene layer at the area not pressed by the mold and tight bonding to the polyethylene terephthalate at the pressed area. Despite the advantages of film-based microfluidic chips, their applications are limited by inherent feedbacks related to these film materials[18–22], such as severe absorption of small nonpolar and weakly polar molecules, adsorption of biomolecules, incompatibility with organic solvents, and leaching of molecules into the microchannels which causes interferences.

Teflon films are an ideal option to overcome the limitations of lab-on-a-film systems due to their exceptional chemical, biological, and physical properties[23–25]. Teflon material, including PTFE (polytetrafluoroethylene), PFA (perfluoroalkoxy), and FEP (fluorinated ethylene-propylene), exhibit superior inertness to almost all chemicals and solvents[26,27], minimal adsorption of molecules, and low molecule leaching[28,29]. PFA and FEP, particularly, are thermoplastic and transparent Teflon, which are highly suitable for fabricating whole-Teflon microfluidic chips. Our research group has pioneered the development of whole-Teflon microfluidic chips and demonstrated their superior properties for microfluidics[30–33]. The fabrication process involves the generation of micropatterns in PFA and FEP slabs (~ 3 mm thick) by hot embossing and thermal sealing of the microchannels. Recent studies have reported the successful formation of micropatterns on Teflon slab substrates through methods such as CNC milling[34,35], nano imprinting[36], water jet machining[37], and laser cutting[38,39]. However, PFA and FEP require accurate temperature control (within an accuracy of several degrees Celsius) and high pressure for chip bonding, causing relatively low successful bonding rates (less than 20%). In addition, the thick nature of these chips brings more challenges: the optical transparency is reduced with a milky white appearance, and the high mechanical stiffness prevents the fabrication of integrated microvalves and the formation of tight-fitting contact with non-flat substrates.

Film-based Teflon microchips are proposed to address the challenges of bulk-based Teflon chips, as they retain the benefits of Teflon while overcoming the drawbacks of bulk-based chips. Thin PFA and FEP films offer high optical transparency[40,41] for on-chip applications such as photochemical reactions and real-time

https://doi.org/10.26434/chemrxiv-2024-vm2pz **ORCID:** https://orcid.org/0000-0001-7898-6736 Content not peer-reviewed by ChemRxiv. **License:** CC BY-NC-ND 4.0

bioanalysis. The excellent physical properties, including the ability to withstand extreme temperatures and UV radiation, enhance the overall stability of the film-based microdevices[42,43]. However, fabricating micropatterns on Teflon films is challenging due to their high melting points and limited available techniques[44,45]. Moreover, chip bonding for the Teflon film-based devices becomes more difficult as the thermoformed shell structure must be protected to prevent the collapse of the micropatterns[46]. For lab-on-a-film systems, connecting the chips to the macroscopic world for fluid delivery is also a critical consideration[47,48]. The traditional approach of fixing a connecting tube or capillary through the accessing hole[49] is impractical for thin-film microfluidic chips. Furthermore, the surface inertness of Teflon materials makes it unfeasible to use adhesive to package the microchips or seal the connection interface[50]. Consequently, there is a need to develop a robust, universal, easy-to-integrate, solvent-resistant, and adhesive-free connector to bridge the chip-to-world interface, particularly for Teflon microfluidic film chips. This is a crucial area that requires attention to fully unlock the potential of lab-on-a-film systems.

This study presents an innovative, low-cost, convenient, and scalable approach for fabricating Teflon-FEP microfluidic film chips. Our approach involves a high-temperature micro embossing technique to pattern FEP thin film adhered to a PDMS support substrate, followed by a fusion bonding method to seal the patterned FEP shell structure with another flat FEP thin film. Additionally, we have developed a robust, universal, adhesive-free connector that ensures stable fluid delivery and demonstrated the easy integration of valves onto the FEP microfluidic film chips. Lastly, we showcase the capabilities of our FEP microfluidic film chips by performing a photochemical reaction, highlighting the chemical resistance and transparency of FEP thin film for organic synthesis. The whole-Teflon thin-film microchips will offer a new microfluidic platform with some distinctive features for various applications: (1) the film chip is highly transparent to visible light and even to UV and IR; (2) the high flexibility makes it easy to form a tight fit to various non-flat surfaces (which can benefit skin sensor and flow chemistry applications, for example); (3) it can be folded to a small volume, increasing the density of microchannels in space; (4) flexible films make it very simple to generate on-chip microvalves; and (5) thin films makes it easy to accurately control temperature on chip. Apparently, these film chips address the limitations of bulk-based Teflon chips while inheriting all the merits of Teflon materials. We believe that this flexible, durable, low-cost, and mass-producible Teflon lab-on-film system will significantly enhance the toolbox of microfluidic technology for research and industrial applications.

2. RESULTS AND DISCUSSIONS

2.1 Fabrication of Teflon-FEP microfluidic film chips

In this study, we developed a novel and cost-effective approach for generating micropatterns on FEP films and bonding the patterned FEP films with flat FEP films to produce FEP microfluidic film chips. Fig. 1 illustrates the whole fabrication process. First, a thin FEP film was attached to a partially cured PDMS substrate that was deformable. The stacking was then placed on a preheated hotplate slightly above the glass transition temperature of FEP (260 ℃). An embossing mold was positioned on the FEP film, and pressure was applied to the steel block above the mold to press the FEP film. This resulted in ladder-shaped micropatterns being formed along with the deformation of the PDMS substrate to match the surface of the embossing mold. Then, we used fusion bonding to create sealed microchannels. Another flat FEP film with access holes was aligned to the patterned FEP films on the PDMS support substrate, and the stacking was clamped using binder clamps. We then heated the stacking in a 250℃ oven for 1 h to bond the FEP films and detached the FEP microfluidic film chips from the PDMS substrate.

Here, the use of the partially cured PDMS support was found to be critical for three reasons: (1) it helped to evenly spread the film without forming creases, ensuring a smooth and uniform surface for the micropatterns to be transferred onto; (2) it greatly facilitated the pattern transfer process by smoothing out any wrinkles that formed and fixing the pattern in the film. Unlike traditional hot embossing for slabs where the pattern is 'etched' into the slab, the film's surface remained smooth after the pattern transfer. Instead, the film was stretched under pressure and high temperature to reshape itself to fit the pattern; (3) during the fully curing process, the reshaped Teflon remained adhered to the PDMS support,

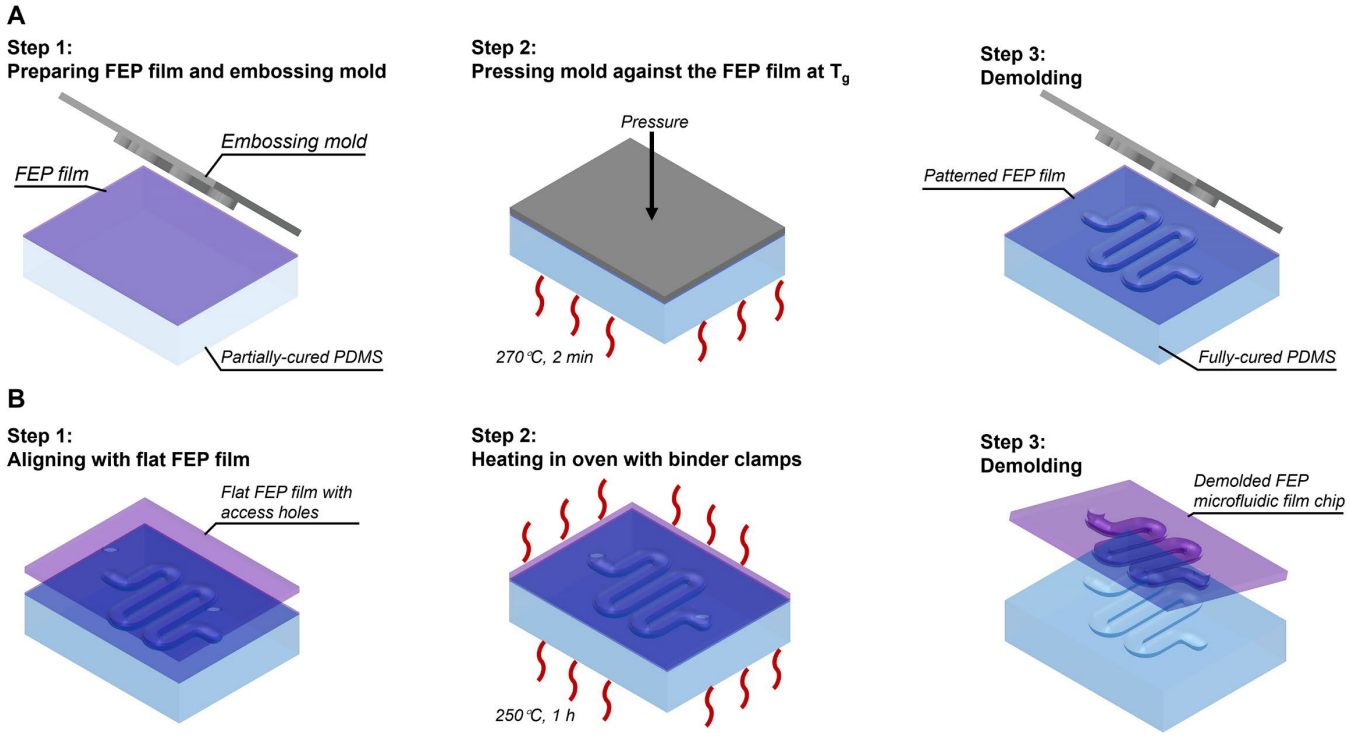

Figure 1. Schematic representation of the fabrication process of microfluidic chips using fluorinated ethylene propylene (FEP) film. (A) Micro embossing for FEP patterns formation. (B) Fusion bonding for microchannel sealing.

https://doi.org/10.26434/chemrxiv-2024-vm2pz ORCID: https://orcid.org/0000-0001-7898-6736 Content not peer-reviewed by ChemRxiv. License: CC BY-NC-ND 4.0

preventing any possible collapse of the film during the subsequent bonding step.

2.1.1 Micro embossing of the FEP films. The first critical step in this method is attaching a 50 μm-thick FEP film to a partially cured PDMS substrate. This specific thickness of FEP film is chosen because it can be embossed while maintaining sufficient mechanical strength to support the embossed structures and prevent collapse.

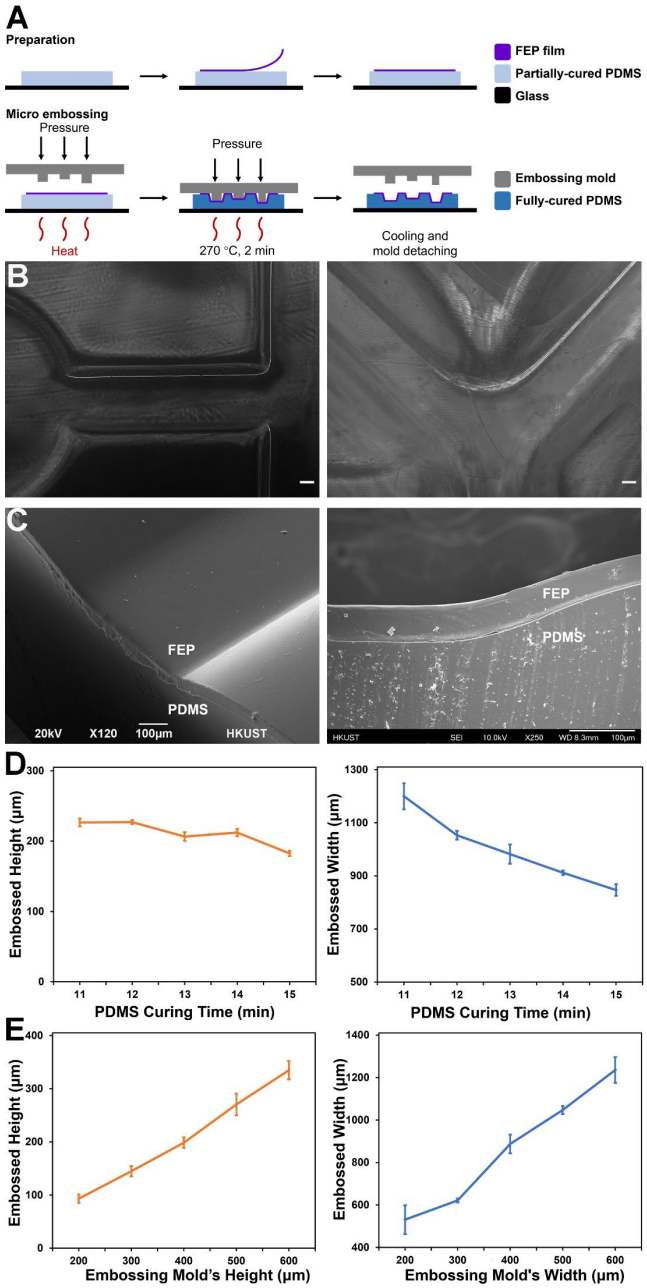

Figure 2. Micropattern formation on FEP films using micro embossing. (A) Schematic of the micro embossing process. (B) Surface topography of the embossed micropatterns on FEP films, and (C) SEM images of the patterned FEP film reserved on the PDMS substrate. (D) Dimensional changes of the FEP micropatterns under different PDMS curing durations. (E) Dimensional changes of the FEP micropatterns under the use of different dimensions of the embossing mold. The scale bars represent 100 μm.

The embossing mold is made of epoxy resin by 3D printing and intermediate molding (see Supporting Information). This positive master possesses high mechanical strength, which enhances the fidelity of the micro embossing process. After complete crosslinking, the epoxy resin attains a hardness of 90 Shore D and a deflection temperature of ~250℃ (Table. S1), ensuring that the embossing mold maintains the microstructures and remains rigid during the pressurization at 270℃. Additionally, the epoxy resin mold has a non-stick surface, making it easy to release from the patterned FEP film.

Fig. 2B and Fig. 2C show the patterned FEP films on the PDMS substrate. The embossed patterns are free of sharp edges or wrinkles, indicating a successful fabrication of different microstructures on the FEP films. During the hot embossing process, the high temperature helps to facilitate the crosslinking of the partially cured PDMS substrate. The elastic modulus and elastic limit of the support substrate increase after complete crosslinking, making it difficult to change the shape of the micropatterns. The use of a fully cured PDMS substrate as a support substrate enables the patterned FEP film to retain its shape after the micro embossing process.

To enhance the effectiveness and versatility of our method, we investigated the impact of PDMS substrates on the cross-sectional profile of microchannels by varying the curing time. When the curing temperature is kept constant, short curing time results in substrates with low elasticity and hardness. Fig. 2D shows that the height of the embossed patterns exhibited minimal change over a curing time ranging from 11 to 14 minutes. Within this curing duration, the PDMS substrate exhibited a low elastic limit and hardness, and the applied medial force was high enough to form micropatterns with maximum depth. We were able to generate FEP micropatterns with a depth above 200 μm under hand-applied pressure, using embossing molds with 400-μm high micropatterns. However, a longer curing time results in a more rigid substrate with high backpressure and resistance during embossing, leading to a shallower embossed depth. The embossed width of a PDMS substrate is determined by its mechanical properties, particularly its elastic modulus and Poisson's ratio. Increasing the curing time from 11 min to 15 min results in a decrease in embossed width due to a higher elastic modulus and lower Poisson's ratio. A curing time of 14 min resulted in improved fidelity of the micro embossing process, with a high embossed depth and small embossed width.

We used a fixed curing time of 14 minutes and varied the dimensions of micropatterns on the embossing mold to produce FEP films with micropatterns of different cross-sectional profiles. The resulting embossed depth was approximately half that of the embossing mold, while the embossed width was more than twice that of the mold, as shown in Fig. 2E. The impact of mold dimensions on the cross-sectional profiles of the FEP micropatterns highlights the potential for designing and fabricating a wide range of micropatterns by selecting embossing molds with different dimensions.

2.1.2 Fusion bonding of the FEP films. The thickness of the flat FEP film used to seal the microchannel is a critical consideration, as soft FEP films with low rigidity and a high thermal expansion coefficient may spontaneously expand and block the microchannel. Flat FEP films with a thickness above 200 μm met our requirements for perfect bonding.

Pressure must be applied between two FEP films to bond them. To prevent the collapse of the microstructures on the FEP films under pressure, we used a fully-cured PDMS support substrate as a holder for the patterned FEP film (Fig. 3A). The micro embossing process enabled the PDMS substrate to form microstructures that precisely matched the patterned FEP films without the need to design and fabricate additional support holder. This straightforward and time-saving method effectively protected the micropatterns on the FEP film from collapsing during bonding.

Additionally, using a PDMS support as the substrate holder improves bonding quality by conformably deforming and distributing pressure evenly to the FEP films, resulting in uniform bonding at the designated sealed area. As shown in Fig. 3B, the patterned FEP films and flat FEP films were effectively fused to form a bonding, with no unbonded areas observed.

Fig. 3E shows the cross-sectional profiles of the bonded microchannel. The heights of the bonded microchannels were

https://doi.org/10.26434/chemrxiv-2024-vm2pz ORCID: https://orcid.org/0000-0001-7898-6736 Content not peer-reviewed by ChemRxiv. License: CC BY-NC-ND 4.0

relatively decreased compared to those of the embossed patterns, while the widths of the bonded microchannels were close to or slightly larger. This is due to the pressure applied to the PDMS support holder during the fusion bonding process, which compressed the PDMS micropatterns medially and expanded them laterally. Our method is suitable for micro embossing using molds with heights above 200 μm, and it can form film-based FEP microchannels with heights below 100 μm. The minimum bottom width of the microchannel fabricated using our method is approximately 500 μm. By designing specific embossing molds and carefully manipulating the substrate properties, we successfully achieved the desired dimensions of the FEP microchannels.

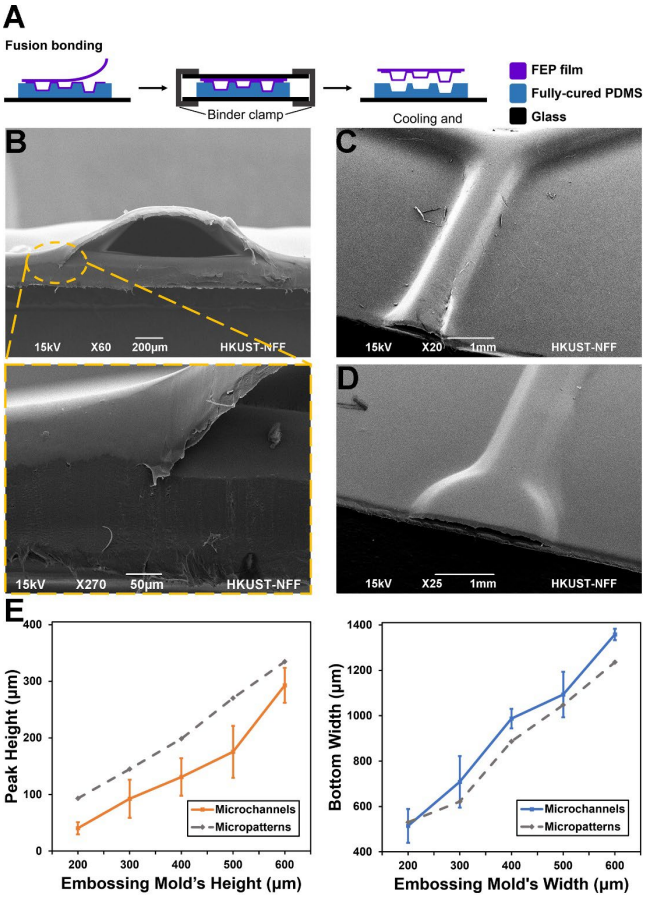

Figure 3. Sealing of FEP film chips using fusion bonding. (A) Schematic of the bonding process to form sealed FEP microfluidic film chips. (B) SEM images of the cross-section of the bonded FEP films and the bonding interface and (C) the bonded FEP microchannel and (D) the bonded FEP microchamber. (E) Dimensional changes of the FEP microchannels under the use of different dimensions of embossing mold.

2.2 Fluid Delivery and Manipulation

2.2.1 Connector for FEP microfluidic film chips. An effective connector is indispensable for all microfluidic chips to bridge microchip fluids with the macroscopic world. Previously, we developed whole-Teflon slab microchips and used epoxy to fix the Teflon tubes inserted into the Teflon slab. However, epoxy cannot stick to Teflon well or withstand organic solvents for a long time, and the microscale thickness of thin films makes it difficult to hold the tubes. To address this issue, we adapted the design of the luer-lock to create a tight-fit, solvent-resistant connector for secure connection between the FEP tubes and the microfluidic film chips. Fig. 4A illustrates the connection mechanism for delivering fluids to FEP microfluidic film chips. Once assembled, the C-shaped chip holder tightly presses the perfluoroelastomer (FFKM) O-ring (on the bottom of the PEEK female luer) against the FEP film chip with its access hole on the top. To accommodate the out-of-plane microstructures of the film chip, we designed a groove on the chip holder to prevent compression of the microchannel by the pressure exerted by the O-ring. The entire connector is made of PEEK, resulting in a leak-proof and solvent-resistant joint between the FEP microchips and the macroscopic world.

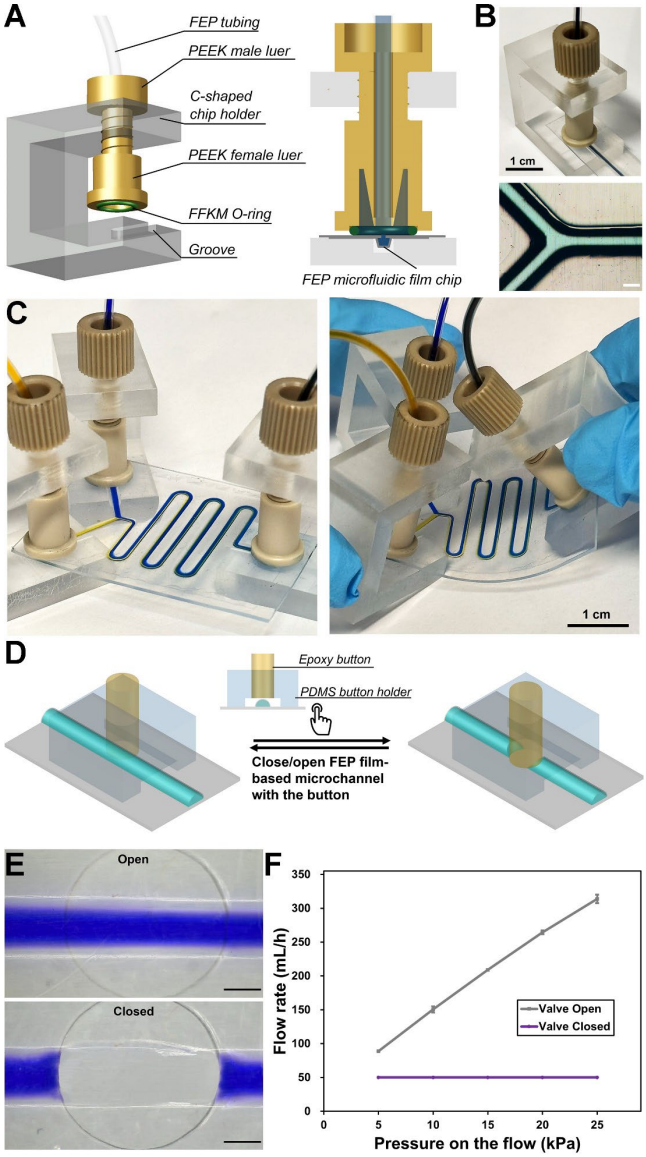

Figure 4. Connector and valve for FEP microfluidic film chips. (A) The mechanism and components of the connector used for FEP microfluidic film chips. (B) Experimental assembly of the connector and delivery of blue chloroform. (C) Mixing of dyed organic solvents in a flexible FEP microfluidic film chip. (D) Schematic of the on-chip 'click' valve function and (E) images of the open and closed status of the valve. (F) Flow rates through the microchannel under different pressure on the flow when the valve is open and closed. The scale bar represents 500 μm.

As shown in Fig. 4B, blue chloroform was delivered to the FEP microfluidic film chips. The microchannel has a bottom width of ~900 μm and a peak height of ~200 μm; the flow rate is set to 150 μL/min, sufficient for scalable organic synthesis. Fig. 4C shows the mixing of hexane and diethyl ether, and we observed no leakage at the connector interface or between the bonded FEP films when we bent the flexible microfluidic film chip.

This robust, reusable, adhesive-free, and universal connector resolves the 'chip-to-world' problem associated with Teflon microfluidic chips. It is space-saving, easy to fabricate and assemble, and adaptable to all film-based microchips. No adhesive is involved in

https://doi.org/10.26434/chemrxiv-2024-vm2pz ORCID: https://orcid.org/0000-0001-7898-6736 Content not peer-reviewed by ChemRxiv. License: CC BY-NC-ND 4.0

the connection, ensuring consistent chemical resistance throughout the whole-Teflon platform. This connector unlocks the potential of FEP microfluidic film chips for stable and long-term organic synthesis applications.

2.2.2 Valve function on FEP microfluidic film chips. The flexibility of the FEP thin film allows for convenient blocking or unblocking of microchannels by applying pressure to the upper arching FEP film. To take advantage of this property, we designed an easy-to-operate 'click' valve and integrated it into our FEP microfluidic film chips, as shown in Fig. 4D. To ensure efficient blocking, the elastic button holder was designed with a smaller hole, with the internal diameter being approximately 100 μm narrower than the button's external diameter, to fix the z-axis position of the button once pressed down. Additionally, the bottom of the button was coated with a thin layer of PDMS (~ 10 μm) to ensure uniform pressure distribution on the FEP film. In Fig. 4E, the button is pressed down by finger to close the Teflon microchannel. The results in Fig. 4F demonstrate that when the 'click' valve is open, the flow in the microchannel is smooth, and the flow rate increases linearly with the driven pressure. Conversely, when the valve is closed, the flow through the microchannel stops, even at high driven pressure (>20 kPa). These results demonstrate that FEP microfluidic film chips provide a simple and efficient strategy for fluid manipulation.

2.3 On-chip Photochemical Synthesis

We demonstrated the application of whole Teflon lab-on-a-film systems for the on-chip photochemical synthesis of the benzylic bromination of 1-indanone (1) using N-brosuccinimide (2) under UV irradiation (Fig. 5A). Benzylic brominations are important reactions in organic chemistry due to their versatility and efficiency in the synthesis of a wide range of compounds, including pharmaceuticals and agrochemicals[51]. The reaction should be carried out under UV-A irradiation (315 ~ 400 nm), which is used widely in photochemical reactions. FEP film in our microfluidic system is ideal for scalable on-chip photochemical reactions due to its high transmittance in this range of UV and resistance to degradation or discoloration under long-term UV irradiation[43,52,53]. The flexibility of the chip allowed for close attachment to the UV light source, improving the efficiency of UV irradiation (Fig. 5B). The distance between the light source and the film was estimated to be 0.5 cm. As illustrated in Fig. 5C, 1-indanone and NBS were injected from two inlets, respectively, and reacted under UV-A irradiation (365 nm). We optimized the inlet flow rates to 5 μL/min each, with a total flow rate of 10 μL/min, to achieve high mixing performance and prolonged residence time under UV exposure. Lower flow rates improve mixing efficiency by prolonging the time for molecular diffusion and increasing the residence time of the mixed reactants under UV exposure within the same distance[54–57], resulting in a complete reaction on the microfluidic chip. The residence time of reactants in our microreactor was calculated to be approximately 136 s under the given flow rate.

Fig. 5D shows the ^{1}H NMR spectrum of the products obtained without and with UV irradiation. The doublet of doublets peaks at 5.6 ppm, which represents No.3 hydrogen, indicates the formation of the target molecule, 3-bromo-1-indanone (3), under UV irradiation. In contrast, no reaction occurred without UV irradiation. This result confirmed the success of the NBS-mediated benzylic bromination reaction under UV irradiation at 365 nm using our FEP microfluidic film chip.

Scaling up the bromination reaction in the batch is challenging due to poor light distribution on large volumes of reactants as dictated by the Beer-Lambert law[58,59]. In contrast, by utilizing our microreactor technology, we achieved high reaction efficiency and obtained a large amount of the desired brominated product by simply operating the microreactor for long periods. Furthermore, we observed that the film-based FEP microfluidic chips used in our microreactor technology significantly improved the yield of the photochemical reaction compared to bulk-based chips. High-performance liquid chromatography (Fig. S3a) revealed the characteristic peaks for the reactant and the product: one at 12.8 min for 1-indanone and another at 14.9 min for the product 3-bromo-1-indanone. Fig. 5E shows that exposing the UV light source from the side of a 50-μm-thick FEP film significantly increases the product signal, while the yield of the product decreases using a bulk-based

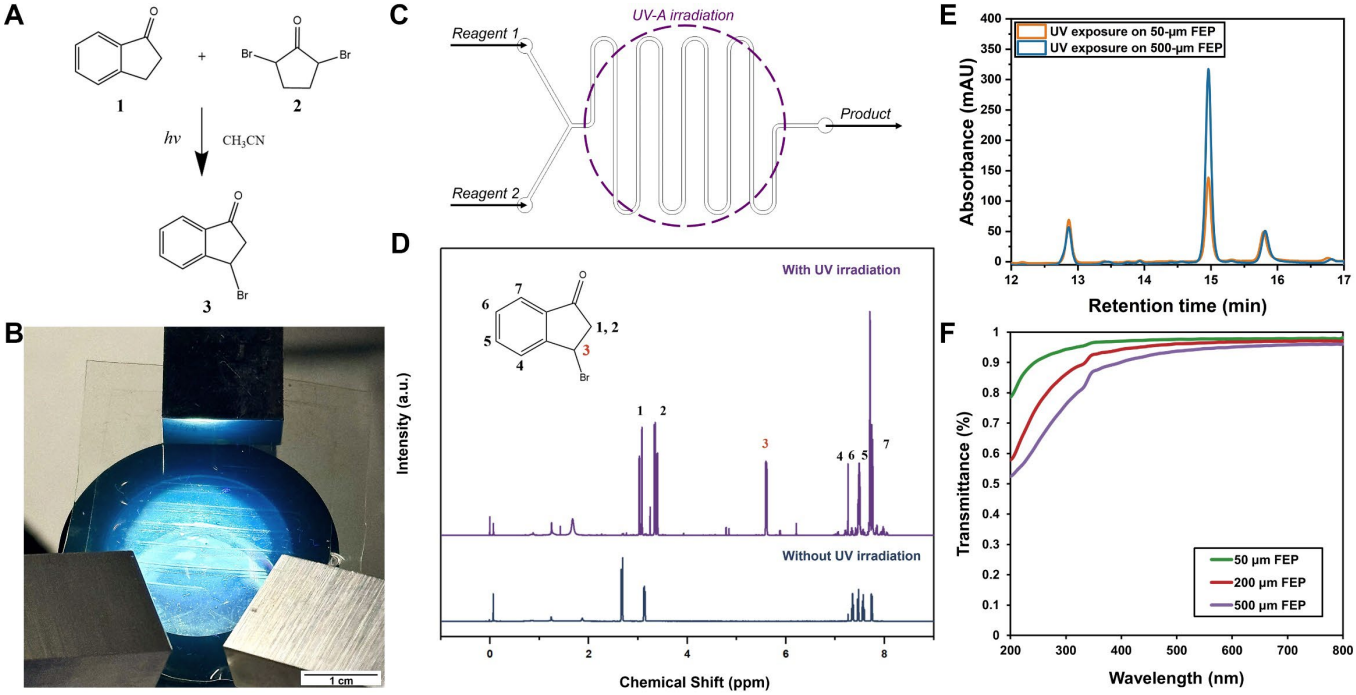

Figure 5. Photochemical reaction in FEP film microreactor. (A) Bromination reaction performed in the FEP film microreactor. (B) Experimental setup of FEP microreactor attached to a UV light source. (C) Schematic of the delivery of the reaction solutions in the FEP microreactor, with details of the chip design and microchannel size provided in Fig. S2. (D) ^{1}H NMR spectra of the synthesized product with and without UV irradiation. (E) HPLC chromatograms of the brominated product by UV exposure on film-based FEP microreactor and bulk-based FEP microreactor. (F) UV-Vis transmittance spectrum of FEP substrates of varying thicknesses.

https://doi.org/10.26434/chemrxiv-2024-vm2pz ORCID: https://orcid.org/0000-0001-7898-6736 Content not peer-reviewed by ChemRxiv. License: CC BY-NC-ND 4.0

chip with a 500-µm-thick FEP plate. This is due to the high transmittance of the FEP thin film to UV light, allowing for more effective UV irradiation on the reagents in the microchannel. We further tested the UV-Vis transmittance of FEP films with different thicknesses (Fig. 5F). A 50-µm-thick FEP film has a transmittance of above 80% to light across the electromagnetic spectrum, including UV, visible, and IR radiation. In the range of UV-A, the FEP thin film in our developed microchips has a transmittance above 90%, while the 500-µm-thick FEP plate used in the bulk-based chips has only ~75% transmittance. Consequently, the yield of the reaction using the FEP thin-film microreactor was 76%, which is significantly higher than the yield in the bulk-based microreactor (57%). The conversion of 1-indanone in the FEP film microreactor was 85%, while the conversion in the bulk-based microreactor was 74%. This result suggests that the thin film inherent in our FEP microfluidic chips can improve the efficiency of on-chip photochemical reactions by allowing for more efficient UV irradiation on the reagents in the microchannel.

3. MATERIALS AND METHODS

3.1 Device Fabrication

3.1.1 Micro embossing of the Teflon-FEP films. We cast a thin layer of the PDMS precursor (approximately 1.5 mm thick) onto a piece of glass using a 10:1 ratio of part A: B. After partially curing the PDMS at 70°C, we carefully adhered a 50-µm-thick FEP film (DAIKIN, Japan) to the surface of the partially cured PDMS substrate. To address the issue of inherent deformation of the FEP films under heat and pressure, corona treatment was applied to the surface of FEP films to increase the surface energy and improve adhesion to the PDMS substrate. After squeezing out any trapped air between the FEP film and the PDMS substrate, we placed the stacking onto a hot plate preheated to 270°C. The prepared epoxy resin mold was tiled onto the FEP film, which was adhered to the PDMS substrate. A 2 kg steel block was placed onto the embossing mold to apply pressure, and the entire stacking was then manually pressed for 2 min. The micropatterns on the epoxy resin mold were simultaneously transferred onto the FEP film and the PDMS substrate. Finally, we allowed the entire stacking to cool down to 80°C while keeping the steel block on the embossing mold. The PDMS substrate with the patterned FEP film on its surface was then demolded from the embossing mold and post-cured at 80°C for 1 h.

3.1.2 Fusion bonding of the FEP microfluidic film chips. Before bonding, we drilled access holes through the flat FEP films for fluid delivery. The surfaces to be bonded were cleaned with acetone and then dried with compressed air. Next, we aligned the flat FEP films to the patterned FEP films on the PDMS support substrate and sandwiched them between two 6-mm thick aluminum plates. We fixed the assembly with four binder clamps and placed it into a 250°C oven for 1 h. After cooling down to room temperature, the FEP films were bonded to each other. We then carefully detached the microfluidic film chips from the PDMS support substrate.

3.2 Investigation of the section profile of the microchannels

To investigate the effect of PDMS substrate crosslinking on patterned FEP films, we used an epoxy resin mold with 400-µm-high and 400-µm-wide micropatterns to produce a series of FEP micropatterns under different curing durations of PDMS at a fixed temperature of 70 °C. We measured the peak heights and bottom widths of the FEP micropatterns under an optical microscope to assess the effect of curing duration, varying it from 11 to 15 min in 1-minute intervals. To further understand the dependence of section profile on the dimensions of the embossing mold, we used a series of embossing molds with square micropatterns with different heights and widths (200 µm, 300 µm, 400 µm, 500 µm, 600 µm) to generate micropatterns on FEP films. We measured the peak heights and bottom widths of the FEP micropatterns and bonded FEP microchannels to assess the effect of mold size. The curing conditions of the PDMS substrate were fixed at 70°C for 14 min.

3.3 Connectors for Teflon Microfluidic Film Chips

We used a C-shaped chip holder and a PEEK luer-lock connector to establish connections between FEP film microchips and the macroscopic world. The chip holder was designed using AutoCAD software and created via CNC milling on PMMA or stainless steel. The FEP tube was inserted through the male luer and screwed into the threaded hole on the chip holder. The male and female luer were then screwed together tightly to create a secure, leak-proof connection between the tubing and the connectors. A 2.2 mm thick perfluoroelastomer O-ring was inserted into the 2-mm-deep groove on the female luer to ensure a leak-free connection between the connectors and the chips. We aligned the C-shaped chip holder with the PEEK luer-lock to the access holes on the microchips and tightened the connectors towards the microchips by screwing the luer-lock.

3.4 On-chip Valve Function

A 'click' valve was used to demonstrate the valve function on the FEP microfluidic film chip. The fabrication and working mechanism of the 'click' valve are shown in Fig. S1. The button used to block the channel was fabricated by double-casting transparent epoxy resin on a 3D-printed mold. We created a holder using PDMS molding on the 3D-printed master to localize the inserted button and fix its position on the z-axis. We injected blue ink into the microchannel from one inlet using a pressure pump. When the valve is open, the holder suspends the button on the surface of the FEP microchannel. To block the channel, the button is released from the holder towards the FEP film by finger. The valve is closed when the button reaches the bottom of the microchannel by squeezing the patterned FEP film onto the flat FEP film. The method used to measure the flow rate under different pressures on the flow is detailed in the Supporting Information.

3.5 On-chip Photochemical Reaction

3.5.1 Photochemical synthesis using FEP microfluidic film chip. Reagents were prepared by dissolving 1-indanone (0.25 M) and N-bromosuccinimide (0.26 M, 1.05 equiv) into acetonitrile, respectively. The solutions were injected into the chip from two inlets through the connectors with FEP tubes. Flow rates were controlled using a syringe pump. A UV light source with a wavelength of 365 nm was positioned close to the mixing element of the chip. The density of the UV power under an irradiation distance of 0.5 cm was estimated to be approximately 6 W/cm^2, and the diameter of the light area was approximately 15 mm. The product was collected at the outlet of the chip into an opaque glass bottle for further analysis.

3.5.2 Characterization of the synthesized product. The HPLC spectrum was utilized to quantify the product present in the reaction mixture. The system is equipped with a Quatpump (Agilent 1100 Series G1311A), a vacuum degasser (Agilent 1100 Series G1322A), an Auto-Sampler (Agilent 1200 Series G1329A), a diode-array detector (DAD, Agilent 1100 Series G1315A), and a reverse phase C18 column (Luna 5 μm C18(2) 100 Å, 250 x 4.6 mm, Phenomenex). The mobile phase consisted of a gradient elution of 5:95 to 100:0 acetonitrile/water with a buffer containing 0.1% trifluoroacetic acid (TFA). The flow rate and injection volume were set at 1 mL/min and 10 μL, respectively.

To confirm the structure of the product, the solution was concentrated using a rotary evaporator. The residue was then treated with 20 mL of diethyl ether and filtered to remove any white precipitate. The organic phase was extracted three times with 10 mL of distilled water each time. The resulting organic phase was dried using anhydrous sodium sulfate and concentrated using a rotary evaporator to yield the desired product, 3-bromo-1-indanone. The ^{1}H NMR spectrum of the product was recorded on a BRUKER AVIII 400 MHz NMR Spectrometer in $CDCl_3$ using tetramethylsilane (TMS; δ =0) as an internal reference.

https://doi.org/10.26434/chemrxiv-2024-vm2pz **ORCID:** https://orcid.org/0000-0001-7898-6736 Content not peer-reviewed by ChemRxiv. **License:** CC BY-NC-ND 4.0

4. CONCLUSIONS

In summary, we have developed a rapid and cost-effective approach for mass-producing whole-Teflon thin film microfluidic chips at a low cost. The micro embossing technique generates micropatterns on FEP thin films, combined with a fusion bonding process with another flat FEP film to form a sealed microchannel. This two-step strategy enables the fabrication of FEP microchannels with designated dimensions with minimal machine requirements. We also demonstrate an effective connector design to ensure a leak-proof and solvent-resistant joint between the Teflon film microchips and external components. Critical components, such as valves, can be easily integrated into the film chips for on-chip fluid manipulation. The whole-Teflon lab-on-a-film platform offers the combined advantages of Teflon materials, such as exceptional solvent resistance, and film-based microsystems, such as remarkable light transmittance (even for UV) and the flexibility to integrate valves. As a proof-of-concept, we performed on-chip photochemical synthesis on the FEP microfluidic film chip and found that the thin-film microchips can improve the yield of the reaction compared to conventional bulk-based chips. We believe this new type of microchip made from Teflon will address the limitations of PDMS and bulk chips, and will find wide applications in organic synthesis, wearable monitoring, and point-of-care testing.

ASSOCIATED CONTENT

Supporting Information: selection of mold materials for micro embossing, preparation of the hot embossing mold, design and fabrication of on-chip 'click' valves, FEP film microreactor for organic synthesis, characterization of the photochemical synthesis.

ACKNOWLEDGMENT

This work was financially supported by Hong Kong Research Grant Council (#16309920, #16300622, and #16309421), Hong Kong ITC (Grant ITC-CNERC14SC01), and Shenzhen Science and Technology Innovation Committee (SZ-SZSTI2010).

REFERENCES

1 G. M. Whitesides, *Nature*, 2006, 442, 368–373.
2 K. S. Elvira, X. C. I Solvas, R. C. R. Wootton and A. J. Demello, *Nat. Chem.*, 2013, 5, 905–915.
3 S. Preetam, B. K. Nahak, S. Patra, D. C. Toncu, S. Park, M. Syväjärvi, G. Orive and A. Tiwari, *Biosens. Bioelectron. X*, 2022, **10**, 100106.
4 M. A. Unger, H. P. Chou, T. Thorsen, A. Scherer and S. R. Quake, *Science (80-.).*, 2000, **288**, 113–116.
5 K. Ren, J. Zhou and H. Wu, *Acc. Chem. Res.*, 2013, **46**, 2396–2406.
6 X. Hou, Y. S. Zhang, G. T. De Santiago, M. M. Alvarez, J. Ribas, S. J. Jonas, P. S. Weiss, A. M. Andrews, J. Aizenberg and A. Khademhosseini, *Nat. Rev. Mater.*, 2017, 2.
7 M. Focke, D. Kosse, C. Müller, H. Reinecke, R. Zengerle and F. Von Stetten, *Lab Chip*, 2010, 10, 1365–1386.
8 G. Jia, J. Siegrist, C. Deng, J. V. Zoval, G. Stewart, R. Peytavi, A. Huletsky, M. G. Bergeron and M. J. Madou, *Colloids Surfaces B Biointerfaces*, 2007, **58**, 52–60.
9 M. Ikeuchi and K. Ikut, in *Micro Electronic and Mechanical Systems*, 2009.
10 G. S. Fiorini and D. T. Chiu, *Biotechniques*, 2005, 38, 429–446.
11 H. Sharma, D. Nguyen, A. Chen, V. Lew and M. Khine, *Ann. Biomed. Eng.*, 2011, **39**, 1313–1327.
12 U. Kloter, H. Schmid, H. Wolf, B. Michel and D. Juncker, in *Proceedings of the IEEE International Conference on Micro Electro Mechanical Systems (MEMS)*, 2004, pp. 745–748.
13 C. Hu, S. Lin, W. Li, H. Sun, Y. Chen, C. W. Chan, C. H. Leung, D. L. Ma, H. Wu and K. Ren, *Lab Chip*, 2016, **16**, 3909–3918.
14 P. Abgrall, C. Lattes, V. Conédéra, X. Dollat, S. Colin and A. M. Gué, *J. Micromechanics Microengineering*, 2006, **16**, 113–121.
15 R. Truckenmüller, S. Giselbrecht, N. Rivron, E. Gottwald, V. Saile, A. Van Den Berg, M. Wessling and C. Van Blitterswijk, *Adv. Mater.*, 2011, **23**, 1311–1329.
16 M. Ikeuchi and K. Ikuta, in *Proceedings of the IEEE International Conference on Micro Electro Mechanical Systems (MEMS)*, 2008, pp. 62–65.
17 M. Ikeuchi and K. Ikuta, *Proc. - IEEE Int. Conf. Robot. Autom.*, 2009, 4469–4472.
18 J. N. Lee, C. Park and G. M. Whitesides, *Anal. Chem.*, 2003, **75**, 6544–6554.
19 G. S. Fiorini, R. M. Lorenz, J. Kuo and D. T. Chiu, *Anal. Chem.*, 2004, **76**, 4697–4704.
20 M. Natali, S. Begolo, T. Carofiglio and G. Mistura, *Lab Chip*, 2008, **8**, 492–494.
21 K. Ren, Y. Zhao, J. Su, D. Ryan and H. Wu, *Anal. Chem.*, 2010, **82**, 5965–5971.
22 Z. Mahmoodi, J. Mohammadnejad, S. Razavi Bazaz, A. Abouei Mehrizi, M. A. Ghiass, M. Saidijam, R. Dinarvand, M. Ebrahimi Warkiani and M. Soleimani, *Drug Deliv. Transl. Res.*, 2019, **9**, 707–720.
23 J. O. Kim, H. Kim, D. H. Ko, K. I. Min, D. J. Im, S. Y. Park and D. P. Kim, *Lab Chip*, 2014, **14**, 4270–4276.
24 J. Pivetal, F. M. Pereira, A. I. Barbosa, A. P. Castanheira, N. M. Reis and A. D. Edwards, *Analyst*, 2017, **142**, 959–968.
25 Y. Shangguan, D. Guo, H. Feng, Y. Li, X. Gong, Q. Chen, B. Zheng and C. Wu, *Macromolecules*, 2014, **47**, 2496–2502.
26 S. G. Newman and K. F. Jensen, *Green Chem.*, 2013, 15, 1456–1472.
27 K. Jähnisch, V. Hessel, H. Löwe and M. Baerns, *Angew. Chemie - Int. Ed.*, 2004, 43, 406–446.
28 W. R. Dolbier, in *Journal of Fluorine Chemistry*, 2005, vol. 126, pp. 157–163.
29 V. Arcella, A. Ghielmi and G. Tommasi, in *Annals of the New York Academy of Sciences*, 2003, vol. 984, pp. 226–244.
30 K. Ren, W. Dai, J. Zhou, J. Su and H. Wu, *Proc. Natl. Acad. Sci. U. S. A.*, 2011, **108**, 8162–8166.
31 B. Shen, B. Xiong and H. Wu, *Biomicrofluidics*, 2015, **9**, 044111.
32 B. Shen and H. Wu, *ACS Sensors*, 2016, **1**, 251–257.
33 Y. Wang, S. Chen, H. Sun, W. Li, C. Hu and K. Ren, *Microphysiological Syst.*, 2018, **1**, 1–1.
34 W. H. Grover, M. G. Von Muhlen and S. R. Manalis, *Lab Chip*, 2008, **8**, 913–918.
35 T. Szymborski, P. Jankowski and P. Garstecki, *Sensors Actuators, B Chem.*, 2018, **255**, 2274–2281.
36 H. Zheng, W. Wang, X. Li, Z. Wang, L. Hood, C. Lausted and Z. Hu, *Lab Chip*, 2013, **13**, 3347–3350.
37 S. Kuhn, T. Noël, L. Gu, P. L. Heider and K. F. Jensen, *Lab Chip*, 2011, **11**, 2488–2492.
38 K. V. Volchetskaya, D. K. Kuznetsov and V. Ya Shur, in *IOP Conference Series: Materials Science and Engineering*, 2019, vol. 699.
39 S. F. Toosi, S. Moradi and S. G. Hatzikiriakos, *Rev. Adhes. Adhes.*, 2017, 5, 55–78.
40 T. Szymborski, P. Jankowski, D. Ogończyk and P. Garstecki, *Micromachines*, 2018, **9**, 1–12.

https://doi.org/10.26434/chemrxiv-2024-vm2pz **ORCID:** https://orcid.org/0000-0001-7898-6736 Content not peer-reviewed by ChemRxiv. **License:** CC BY-NC-ND 4.0

41 Y. Jiang, G. Wu, Y. Li and W. Wu, *RSC Adv.*, 2019, **9**, 2650–2656.

42 X. Zhang, J. Hillenbrand, G. M. Sessler, S. Haberzettl and K. Lou, *Appl. Phys. A Mater. Sci. Process.*, 2012, **107**, 621–629.

43 X. Ma, C. Song, F. Zhang, Y. Dai, P. He and X. Zhang, *ACS Appl. Mater. Interfaces*, 2022, **14**, 51291–51300.

44 T. W. De Haas, H. Fadaei and D. Sinton, *Lab Chip*, 2012, **12**, 4236–4239.

45 D. Flachs, F. Emmerich, G. L. Roth, R. Hellmann and C. Thielemann, in *Journal of Physics: Conference Series*, 2019, vol. 1407.

46 Q. Liu, Y. Liu, F. Wu, X. Cao, Z. Li, M. Alharbi, A. N. Abbas, M. R. Amer and C. Zhou, *ACS Nano*, 2018, **12**, 1170–1178.

47 S. Miserere, G. Mottet, V. Taniga, S. Descroix, J. L. Viovy and L. Malaquin, *Lab Chip*, 2012, **12**, 1849–1856.

48 Y. Temiz, R. D. Lovchik, G. V. Kaigala and E. Delamarche, *Microelectron. Eng.*, 2015, **132**, 156–175.

49 Y. C. Tsai, S. J. Yang, H. T. Lee, H. P. Jen and Y. Z. Hsieh, *J. Chinese Chem. Soc.*, 2006, **53**, 683–688.

50 A. A. S. Bhagat, P. Jothimuthu, A. Pais and I. Papautsky, *J. Micromechanics Microengineering*, 2007, **17**, 42–49.

51 D. Cantillo, O. De Frutos, J. A. Rincon, C. Mateos and C. Oliver Kappe, *J. Org. Chem.*, 2014, **79**, 223–229.

52 Z. Liu, Y. Huang, Y. Shi, X. Tao, H. He, F. Chen, Z. X. Huang, Z. L. Wang, X. Chen and J. P. Qu, *Nat. Commun.*, 2022, **13**, 4083.

53 M. Dilla, A. E. Becerikli, A. Jakubowski, R. Schlögl and S. Ristig, *Photochem. Photobiol. Sci.*, 2019, **18**, 314–318.

54 Z. Wang, X. Yan, Q. Zhou, Q. Wang, D. Zhao and H. Wu, *Anal. Chem.*, 2023, **95**, 8850–8858.

55 J. C. M. Monbaliu and J. Legros, *Lab Chip*, 2022, 23, 1349–1357.

56 M. B. Plutschack, B. Pieber, K. Gilmore and P. H. Seeberger, *Chem. Rev.*, 2017, 117, 11796–11893.

57 L. Liu, P. Liu, D. Zhang, H. Y. Zhang, Y. Zhang and J. Zhao, *ACS Omega*, 2022, **7**, 4624–4629.

58 D. Cambié, C. Bottecchia, N. J. W. Straathof, V. Hessel and T. Noël, *Chem. Rev.*, 2016, 116, 10276–10341.

59 D. Cantillo and C. O. Kappe, *React. Chem. Eng.*, 2017, 2, 7–19.

https://doi.org/10.26434/chemrxiv-2024-vm2pz **ORCID:** https://orcid.org/0000-0001-7898-6736 Content not peer-reviewed by ChemRxiv. **License:** CC BY-NC-ND 4.0

5. FOR TABLE OF CONTENTS ONLY

https://doi.org/10.26434/chemrxiv-2024-vm2pz **ORCID:** https://orcid.org/0000-0001-7898-6736 Content not peer-reviewed by ChemRxiv. **License:** CC BY-NC-ND 4.0